The Retrieval Method of Effective Parameters for Acoustic Metamaterials

Temirlan Ismagulov

Nazarbayev University

May 2, 2025

Supervisor: Professor Bakhtiyar Orazbayev

Department of Physics

The Retrieval Method of Effective Parameters for Acoustic Metamaterials*

Temirlan Ismagulov

May 5, 2025

Abstract

Efficient, broadband characterization of acoustic metamaterials is essential for translating their extraordinary wave-manipulation capabilities into practical devices. Here we present a robust retrieval framework that extracts key effective parameters directly from two-port scattering measurements acquired in a 1D circular waveguide: acoustic impedance Z_{eff}, refractive index n_{eff}, dynamic mass density ρ_{eff}, and dynamic Young's modulus E_{eff}. The expressions for effective parameters are obtained using reflection and transmission through a homogeneous slab by summing the infinite series of internal multiple reflections. A Kramers-Kronig branch selection rule is then implemented to enforce passivity and continuity of n_{eff} across frequency, eliminating ambiguity in the complex-logarithm inversion. The proposed method provides a fast route to quantify dispersive parameters in acoustic metamaterials, offering a valuable tool for the design of cloaks, lenses, and noise-control elements.

*I thank Physics Faculty, particularly Prof. Bakhtiyar Orazbayev, for support in thesis writing

Contents

List of Figures

I. INTRODUCTION

Acoustic metamaterial research (1; 2) has attracted considerable attention over the last two decades. Despite impressive progress, the community is still debating the fundamental validity of the *effective-medium* concept, which is indispensable for understanding wave propagation in both electromagnetic and acoustic metamaterials (3; 4).

Artificially structured acoustic metamaterials exihibit interesting properties - negative refraction, total transmission, and acoustic cloaking – that have no analogy in conventional materials(5). A holistic description of these kind of media is based on scattering matrices (*S-matrices*) that relate incident and outgoing waves and provide a crucial information to retrieve effective parameters (acoustic impedance, refractive index, effective mass density, and bulk modulus) (6; 7).

This thesis investigates acoustic scattering in a circular waveguide with and without embedded scatterers. We particularly research Helmholtz resonators – a bottle-like cavities producing sharp monopolar resonances and deep local band gaps (8; 9). By inserting a single or an array of resonators inside the tube, we study the distribution of the acoustic pressure field, resonance frequencies, and the global S matrix.

Our primary objective is to experimentally extract the reflection (S_{11}, S_{22}) and transmission (S_{12}, S_{21}) coefficients and to deduce the corresponding effective impedance Z_{eff} and refractive index n_{eff} using theoretical approach for electromagnetic and acoustic waves(10; 11). Thus, we employ a two-port waveguide equipped with calibrated loudspeakers and multiple microphones(12). By exciting each port separately and recording complex pressures at different coordinates, we find out forward and backward travelling wave amplitudes, build the full *S-matrix*, and compare the results with transfer-matrix predictions and finite-element models.

Besides providing a robust protocol for resonance characterization in confined geometries, the methodology developed here clarifies the range of validity of effective-medium descriptions for strongly resonant structures and paves the way for rational design of broadband acoustic devices—including silencers, filters, and duct cloaks—based on metamaterial principles.

II. BACKGROUND

A central challenge in characterising metamaterials is the retrieval of effective parameters: acoustic impedance Z, refractive index n, effective density ρ_{eff} and Young modulus E_{eff}. The microwave Nicolson-Ross-Weir (NRW) technique was first adapted to resonant structures by Chen *et al.* (13) and generalised to inhomogeneous composites by Smith *et al.* (14). Subsequent variants enforce passivity (15) or fit causal dispersion models (16), but all face the multivalued–logarithm "branch" problem for n. Szabó *et al.* (17) introduced a practical solution: use discrete Kramers–Kronig integrals to estimate $\Re\{n\}$ from the unambiguous $\Im\{n\}$, then select the integer branch m that minimizes the difference between both values. Closed–form KK inversions have since been proposed for THz (18) and acoustic metasurfaces (19), but have not yet been combined with duct S–matrix measurements—the gap addressed in this thesis. Experimental demonstrations of negative effective density or modulus relied on locally resonant monopoles/dipoles (Helmholtz cavities, membranes, coated spheres). Pioneering work by Fang *et al.* (20), Li & Chan (21) and Fokin *et al.* (22) triggered systematic retrieval studies, e.g. hollow silicone cylinders with KK branch selection (22). Surface–resonant waves in such media enable sub–diffraction imaging (23) and broadband barriers (24). For samples inserted in a 1-D duct, four-microphone methods provide complex S_{11}, S_{21} without plane-wave assumptions (25; 26). Parazzoli *et al.* (27) and Menzel *et al.* (28) described de-embedding to an internal reference plane, permitting intrinsic R, T coefficients even for anisotropic slabs.

III. MOTIVATION

Three unresolved issues motivate the present study:

1. **Branch continuity.** Thick or highly lossy slabs exhibit multiple m–branches. In this study we want to demonstrate it (17).

2. **Holistic Retrieval Method.** Basically, there is no general approach to derive effective parameters with resolving branching issues. In this work, we want to prepare thorough approach of doing it.

3. **Design Metamaterials** This study is also aimed to research properties of basic acoustic metamaterials. We want to introduce the general principles of designing metamaterials (17).

This thesis addresses these gaps by deriving KK-guided analytic formulas for acoustic slabs, implementing a robust Python code for branch selection, and validating the method on single- and multi-resonator wave-guide experiments.

IV. METHODOLOGY

IV.1. Retrieval of Scattering Matrix

To study the properties of a given acoustic metamaterial, the experiments are carried out in a 1D acoustic waveguide, a device designed to guide and control the propagation of acoustic waves through a confined path. 1D acoustic waveguide in our study looks like a cylindrical tube with 4 microphones placed along the waveguide and 2 speakers at the end of each side, as shown in Figure 1. Then, each speaker is turned on separately to study the readings of microphones. The microphones itself measure pressure at a given point throughout the study. The given information from each speaker separately is not sufficient to reveal crucial information about an acoustic material placed inside. Thus, the combination of all the data from each microphone can be utilized to derive scattering matrix.

(a) Left Speaker Activated

(b) Right Speaker Activated

Figure 1: 1D Acoustic Waveguide Working Principle

The scattering matrix, often denoted as the S-matrix, offers a comprehensive description of the interplay between incoming and outgoing waves in the system with several ports. Each row and column within this matrix signifies distinct input and output channels. A system can be described as an n-port, with each "port" signifying the origin or destination of the sound. Elements of the S-matrix are called S parameters and are shown in Figure 4. The scattering matrix S connects the outgoing and incoming waves by the following formula

$$\vec{B} = S\vec{A}, \tag{1}$$

where $\vec{A}$ is referring to the incoming waves and $\vec{B}$ is referring to the outgoing waves.

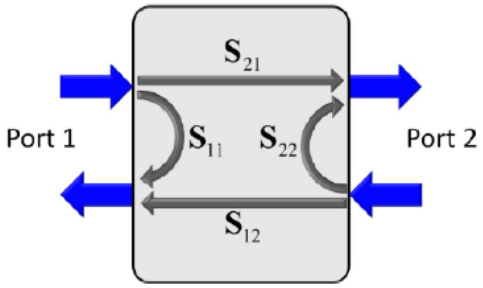

Figure 2: Scattering Matrix

$$\begin{bmatrix} B_1 \\ B_2 \end{bmatrix} = \begin{bmatrix} S_{11} & S_{12} \\ S_{21} & S_{22} \end{bmatrix} \begin{bmatrix} A_1 \\ A_2 \end{bmatrix}. \tag{2}$$

In the ideal system conditions, if no scatter is placed in the duct there will be no reflection parameters, so the S-matrix will look this way

$$\begin{bmatrix} S_{11} & S_{12} \\ S_{21} & S_{22} \end{bmatrix} = \begin{bmatrix} 0 & 1 \\ 1 & 0 \end{bmatrix}. \tag{3}$$

Therefore, we can extract the scattering matrix from vectors $\vec{A}$ and $\vec{B}$.

$$S = \frac{\vec{B}}{\vec{A}} \tag{4}$$

Hence, we need to extract vectors $\vec{A}$, $\vec{B}$. The next set of equations will describe the pressures measured from the excitation from the first and second ports respectively. A_{ij} and B_{ij} letters denote amplitudes of incoming and outgoing waves respectively. So, the amplitude of pressure recorded by microphones in P_{ij} (i denotes the position of a microphone and j denotes the speaker excited). Hence, the equation for pressure at each microphone can be written using

wave amplitudes as

$$\begin{cases} P_{11} = A_{11}e^{-ikx_1} + B_{11}e^{ikx_1} \\ P_{21} = A_{11}e^{-ikx_2} + B_{11}e^{ikx_2} \\ P_{31} = A_{21}e^{-ikx_3} + B_{21}e^{ikx_3} \\ P_{41} = A_{21}e^{-ikx_4} + B_{21}e^{ikx_4}. \end{cases} \tag{5}$$

Now, we can write the equation in vector form to solve it further. Let us introduce A and B vectors.

$$\vec{A_1} = \begin{bmatrix} A_{11} \\ A_{21} \end{bmatrix}, \quad \vec{B_1} = \begin{bmatrix} B_{11} \\ B_{21} \end{bmatrix}, \quad \vec{A_2} = \begin{bmatrix} A_{12} \\ A_{22} \end{bmatrix}, \quad \vec{B_1} = \begin{bmatrix} B_{12} \\ B_{22} \end{bmatrix}, \tag{6}$$

Then, pressure can also be written in matrix form. Let us also introduce the m matrix.

$$\vec{P_1} = \begin{bmatrix} P_{11} \\ P_{21} \\ P_{31} \\ P_{41} \end{bmatrix}, \quad \vec{P_1} = \begin{bmatrix} P_{12} \\ P_{22} \\ P_{32} \\ P_{42} \end{bmatrix}, \quad m = \begin{bmatrix} e^{-ikx_1} & e^{ikx_1} & 0 & 0 \\ e^{-ikx_2} & e^{ikx_2} & 0 & 0 \\ 0 & 0 & e^{-ikx_3} & e^{ikx_3} \\ 0 & 0 & e^{-ikx_4} & e^{ikx_4} \end{bmatrix}. \tag{7}$$

Combining the expressions give us

$$\overrightarrow{AB}_1 = \begin{bmatrix} \vec{A}_1 \\ \vec{B}_1 \end{bmatrix}, \quad \overrightarrow{AB}_2 = \begin{bmatrix} \vec{A}_2 \\ \vec{B}_2 \end{bmatrix}, \quad \begin{cases} \vec{P}_1 = m \cdot \overrightarrow{AB}_1 \\ \vec{P}_2 = m \cdot \overrightarrow{AB}_2. \end{cases} \tag{8}$$

Solving the equation 8 and placing the values $\vec{A}$ and $\vec{B}$ in the expression 4 give the S matrix.

IV.2. Helmholtz Resonators

As a scattering medium in experiment, we use Helmholtz resonators. A Helmholtz resonator is an example of a scatter, effectively dispersing acoustic waves. In terms of its geometry, it comprises a neck connected to a cavity. Resonance in a Helmholtz resonator occurs when an incoming sound wave possesses a frequency that closely matches the resonant frequency of the device's neck. Conceptually, the Helmholtz resonator is similar to a mass-spring system, where an attached mass undergoes oscillation in response to a periodic external force. In the case of the Helmholtz resonator, a specific volume of air with a designated mass experiences

oscillation within the neck. The frequency at which a Helmholtz resonator operates might

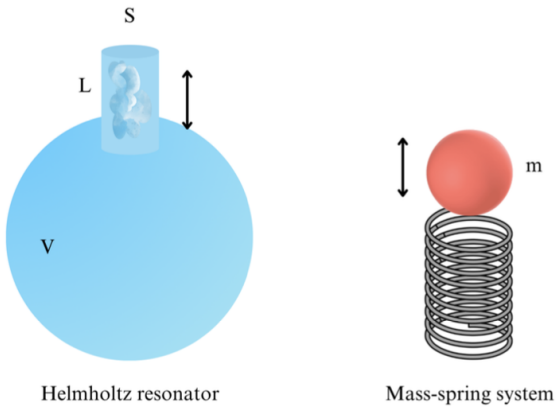

Figure 3: Helmholtz Resonators Working Principle

be found by the following formula

$$f = \frac{c}{2\pi}\sqrt{\frac{S}{V\,L}}, \tag{9}$$

where f - resonance frequency (Hz), c - speed of sound in air (m/s), S - neck cross–sectional area (m^2), V - cavity volume (m^3), L - neck length (m).

IV.3. Reflection and Transmission

Waves inside an acoustic metamaterial slab undergo multiple reflections and transmissions. So, the values in the S matrix observed are the result of the infinite sum of waves from each side. We assume that a normally incident wave propagates inside a homogeneous slab of thickness d_{eff}. As a reference wave vector k_0 we denote wave vector of air and for the slab it is k_{eff}.

To express multiple reflection in terms of two medium parameters, we have to derive reflection and transmission coefficients for a single propagation. Imposing boundary conditions at point $x = 0$

$$\begin{cases} \psi_0 e^{ik_0 x_0} + \psi_r e^{-ik_0 x_0} = \psi_t e^{ik_{\text{eff}} x_0} \\ k_0\left(\psi_0 e^{ik_0 x_0} - \psi_r e^{-ik_0 x_0}\right) = k_{\text{eff}}\psi_t e^{ik_{\text{eff}} x_0}. \end{cases} \tag{10}$$

Similarly, imposing boundary conditions at point $x = d_{eff}$ yeilds

$$\begin{cases} \psi_t e^{ik_{\text{eff}}d_{\text{eff}}} + \psi_{r2} e^{-ik_{\text{eff}}d_{\text{eff}}} = \psi_{t2} e^{ik_0 d_{\text{eff}}} \\ k_{\text{eff}}\psi_t e^{ik_{\text{eff}}d_{\text{eff}}} - k_{\text{eff}}\psi_{r2} e^{-ik_{\text{eff}}d_{\text{eff}}} = k_0 \psi_{t2} e^{ik_0 d_{\text{eff}}} \end{cases} \tag{11}$$

Solving equation 10 using $r = \frac{\psi_r}{\psi_0}$ and $t = \frac{\psi_t}{\psi_0}$ gives us

$$t = \frac{2k_0}{k_0 + k_{eff}}, \quad r = \frac{k_0 - k_{eff}}{k_0 + k_{eff}}. \tag{12}$$

Similarly, solving equation 11 obtains the following

$$t' = \frac{2k_{\text{eff}}}{k_0 + k_{\text{eff}}} \quad r' = \frac{k_0 - k_{\text{eff}}}{k_0 + k_{\text{eff}}} \cdot e^{2ik_{\text{eff}}d} \tag{13}$$

Substituting acoustic impedance in equations 12 and 13 provides

$$t = \frac{2Z_{\text{eff}}}{Z_{\text{eff}} + Z_0}, \quad \text{and} \quad r = \frac{Z_{\text{eff}} - Z_0}{Z_{\text{eff}} + Z_0} \quad . \tag{14}$$

The net reflection coefficient R at the first interface results from the sum of the following terms:

1. The first reflection from the air–slab interface:

$$R_0 = r\,. \tag{15}$$

2. The wave transmitted into the slab, reflected at the second interface, and then transmitted back to the interface:

$$R_1 = t\, r_{23}\, t'\, e^{-2i\, n_{\text{eff}} k_0 d}\,, \tag{16}$$

   where for a symmetric ambient $r_{23} = \frac{Z_{\text{air}} - Z_{\text{eff}}}{Z_{\text{air}} + Z_{\text{eff}}} = -r$.

3. Subsequent terms represent additional internal round-trips and have the form

$$R_m = t\, r_{23}\, (r_{21}\, r_{23})^{m-1}\, t'\, e^{-2im\, n_{\text{eff}} k_0 d} \quad (m \geq 1)\,. \tag{17}$$

Because r_{21} (reflection from inside the slab at the first interface) equals r_{23} in magnitude, the common ratio of the geometric series is $r^2 e^{-2i\,n_{\text{eff}}k_0 d}$. Thus, the total reflection is:

$$\begin{aligned} R &= r + t\,t'\,r\,e^{-2i\,n_{\text{eff}}k_0 d} \sum_{m=0}^{\infty} \left(r^2 e^{-2i\,n_{\text{eff}}k_0 d}\right)^m \\ &= r + \frac{t\,t'\,r\,e^{-2i\,n_{\text{eff}}k_0 d}}{1 - r^2 e^{-2i\,n_{\text{eff}}k_0 d}}\,. \end{aligned} \tag{18}$$

Since

$$t\,t' = \frac{2Z_{\text{eff}}}{Z_{\text{eff}} + Z_{\text{air}}} \cdot \frac{2Z_{\text{air}}}{Z_{\text{eff}} + Z_{\text{air}}} = \frac{4Z_{\text{eff}}Z_{\text{air}}}{\left(Z_{\text{eff}} + Z_{\text{air}}\right)^2}\,, \tag{19}$$

one may also express R as

$$\boxed{R = \frac{r\left(1 - e^{-2i\,n_{\text{eff}}k_0 d}\right)}{1 - r^2 e^{-2i\,n_{\text{eff}}k_0 d}}\,.} \tag{20}$$

Similarly, the overall transmission coefficient T is obtained by summing all transmitted contributions:

$$\begin{aligned} T &= t\,t'\,e^{-i\,n_{\text{eff}}k_0 d} \sum_{m=0}^{\infty} \left(r^2 e^{-2i\,n_{\text{eff}}k_0 d}\right)^m \\ &= \frac{t\,t'\,e^{-i\,n_{\text{eff}}k_0 d}}{1 - r^2 e^{-2i\,n_{\text{eff}}k_0 d}}\,. \end{aligned} \tag{21}$$

Thus,

$$\boxed{T = \frac{\dfrac{4Z_{\text{eff}}Z_{\text{air}}}{\left(Z_{\text{eff}} + Z_{\text{air}}\right)^2}\,e^{-i\,n_{\text{eff}}k_0 d}}{1 - \left(\frac{Z_{\text{eff}} - Z_{\text{air}}}{Z_{\text{eff}} + Z_{\text{air}}}\right)^2 e^{-2i\,n_{\text{eff}}k_0 d}}\,.} \tag{22}$$

IV.4. Extraction of Z_{eff} and n_{eff}

Once the intrinsic (de-embedded) reflection R and transmission T coefficients are determined (for example, from measured S_{11} and S_{21}), one may invert the above equations to solve for Z_{eff} and n_{eff}. A commonly used inversion procedure is as follows:

Effective Impedance Z_{eff}. One standard inversion formula is

$$\boxed{Z_{\text{eff}} = Z_{\text{air}}\,\frac{1 - R^2 + T^2 + \sqrt{\left(1 - R^2 + T^2\right)^2 - 4T^2}}{2R}\,.} \tag{23}$$

The square root is chosen such that $\Re\{Z_{\text{eff}}\} > 0$.

Effective Refractive Index n_{eff}. An auxiliary variable is defined by

$$X = \frac{1 - R^2 + T^2 + \sqrt{(1 - R^2 + T^2)^2 - 4T^2}}{2T}\,. \tag{24}$$

Since the transmission coefficient for a homogeneous slab is given by

$$T = \frac{4Z_{\text{eff}} Z_{\text{air}} e^{-i\, n_{\text{eff}} k_0 d}}{(Z_{\text{eff}} + Z_{\text{air}})^2 \left[1 - r^2 e^{-2i\, n_{\text{eff}} k_0 d}\right]}\,, \tag{25}$$

one may relate the phase accumulation in the slab to X and obtain

$$e^{-i\, n_{\text{eff}} k_0 d} = X\,. \tag{26}$$

Taking the logarithm (and accounting for the multivalued nature of the complex logarithm), we have

$$-i\, n_{\text{eff}} k_0 d = \ln\Big(X\Big) \quad \Longrightarrow \quad \boxed{n_{\text{eff}} = \frac{-i}{k_0 d} \ln(X) + \frac{2\pi m}{k_0 d}\,,} \tag{27}$$

where m is an integer chosen so that n_{eff} is continuous in frequency and compatible with passivity conditions (typically $\Im\{n_{\text{eff}}\} \geq 0$ in acoustics, depending on the time-harmonic convention).

IV.5. Incorporating Causality via KK Relations

The KK relations are a direct consequence of causality and relate the real and imaginary parts of any analytic response function. The approach in Szabo (17) uses these relations to calculate the real part of the effective refractive index from its imaginary part. This extra step is crucial to uniquely fix the branch of the complex logarithm. In the derivation, after writing the preliminary extraction formula

$$n_{\text{eff}} = \frac{-i}{k_0 d} \ln\left(X\right) + \frac{2\pi m}{k_0 d}, \tag{28}$$

the KK integral is evaluated to obtain an approximation for the real part of n_{eff}. The branch number is then selected such that

$$m = \text{Round}\left(\frac{n_{\text{KK}} - n_{\text{eff}}^{\prime(0)}}{2\pi/(k_0 d)}\right), \tag{29}$$

where n_{KK} is the refractive index estimated from the KK relation, and $n_{\text{eff}}^{\prime(0)}$ is the principal value from the logarithm. This guarantees that the retrieved n_{eff} is not only continuous but also consistent with causality.

IV.6. Extraction of Effective Density ρ_{eff} and Young Modulus E_{eff}

The NRW–type retrieval described in the previous subsection yields the effective acoustic impedance $Z_{\text{eff}}(\omega)$ and the effective refractive index $n_{\text{eff}}(\omega) = n'(\omega) + \mathrm{i}\, n''(\omega)$ of the homogeneous slab. In acoustics these two complex functions are sufficient to recover the fundamental material constants: the dynamic mass–density ρ_{eff} and Young modulus E_{eff}.

By definition $n_{\text{eff}} = c_0/c_{\text{eff}}$, where c_0 is the sound velocity in the reference medium (air in our experiments) and c_{eff} is the complex phase velocity inside the effective medium.

$$c_{\text{eff}} = \frac{c_0}{n_{\text{eff}}}. \tag{30}$$

Complex Density. For plane-wave motion in a homogeneous medium the specific impedance is $Z = \rho\, c$. Consequently

$$\rho_{\text{eff}} = \frac{Z_{\text{eff}}}{c_{\text{eff}}} = \boxed{Z_{\text{eff}}\,\frac{n_{\text{eff}}}{c_0}}. \tag{31}$$

Equation (31) shows that ρ_{eff} inherits both the dispersion and the losses (through Z_{eff} and n_{eff}) of the metamaterial.

Young modulus. Inserting (30) and (31) we obtain

$$\begin{aligned} E_{\text{eff}} \;=\; K_{\text{eff}} &= \rho_{\text{eff}}\, c_{\text{eff}}^2 = \frac{Z_{\text{eff}}\, n_{\text{eff}}}{c_0}\,\left(\frac{c_0}{n_{\text{eff}}}\right)^2 \\ &= \boxed{\frac{Z_{\text{eff}}\, c_0}{n_{\text{eff}}}}. \end{aligned} \tag{32}$$

Equations (31) and (32) are the closed-form expressions that convert the retrieved pair $\{Z_{\text{eff}}, n_{\text{eff}}\}$ into the physically more intuitive pair $\{\rho_{\text{eff}}, E_{\text{eff}}\}$. Both results are complex-valued: their imaginary parts represent viscous and thermal losses or local-resonant dispersion in the metamaterial.

IV.7. Simulations

It is necessary to verify the applicability of the theory and the code. Thus, we have implemented the COMSOL program in the study to simulate acoustic physics in the 1D waveguide. In Figure 8 the pressure acoustics simulations in the COMSOL program are shown.

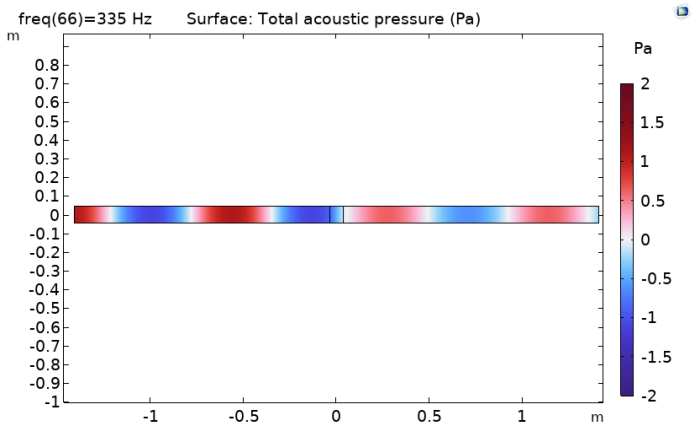

Figure 4: COMSOL Simulation Setup

The Lorentz-type material is a model that involves modeling a material as a dispersive medium. The equation of effective acoustic impedance in Lorentz-type material is as in equation 33. It introduces the dispersion in a slab, so we can study effective properties in a more material than air. In addition, this kind of material is essential to avoid the Fabri-Perot resonance that might occur due to the multiple wave overlap. Hence, we expect to observe that the effective impedance graph to be consistent with equation33.

$$\tilde{Z}(\omega) = Z_\infty + \frac{\left(Z_s - Z_\infty\right)\omega_t^2}{\omega_t^2 - \omega^2 + i\,\Gamma_0\,\omega} \tag{33}$$

(a) 1D Acoustic Waveguide

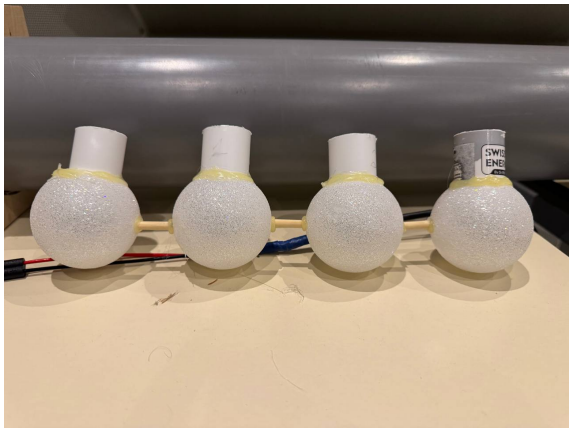

(b) Helmholtz Resonators

Figure 5: Experimental Setup

IV.8. Experimental Design

The experimental setup given in the Figure 5 below. As seen in Figure 5(a), we built cylindrical two halves of the acoustic waveguide, so we can easily place resonators at the center of it. One might also notice that we run experiments in an acoustic chamber, known as "silent room", where the most of the sound waves are absorbed to minimize noise.

In addition, we have prepared the same resonators (resonant frequency $\approx$ 580Hz) to simulate effective media that replicate a locally resonant structure. To recreate this kind of meta-material, we connected two, three, and four resonators at a close distance to each other, particularly 2cm. So, by changing the number of resonators in this array, we can control the properties of the effective medium. The more resonators present in the array, the bigger "gap" we should observe in the S matrix graph. This suggests that the array of resonators will not behave as a single resonator anymore.

V. RESULTS

V.1. Simulations

Thus, we have made two simulations that can provide insights into the validity of theory. First, we simulated free run with no slab placed in the waveguide. It is clear that in this kind of simulations there should be constant Z_{eff} and n_{eff}. So, it means that the results must be the same as for the air. As seen in Figure 6, the results are accurate and match expected theoretical predictions.

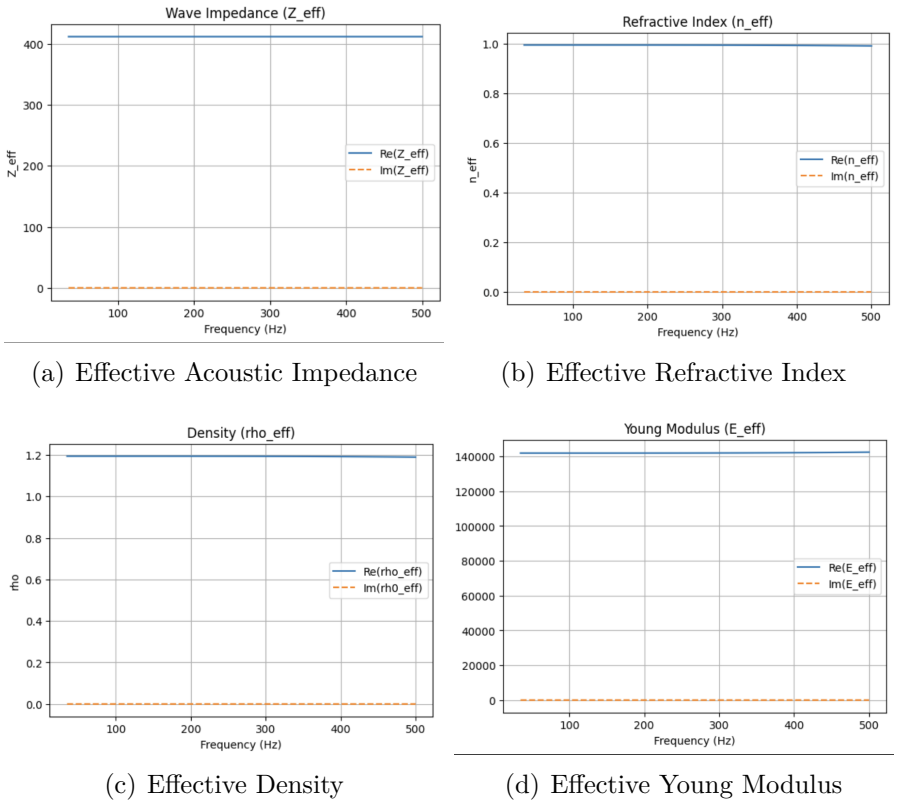

(a) Effective Acoustic Impedance (b) Effective Refractive Index

(c) Effective Density (d) Effective Young Modulus

Figure 6: Simulation with No Slab

Conversely, the simulations with Lorentz-type material must demonstrate dispersive properties. We have to observe the change in both Z_{eff} and n_{eff} according to the Lorentz-type dispersion. The acoustic impedance in this run should be consistent with equation 33. More importantly, we have to notice branching issue for n_{eff}. In Figure 7, there are represented results for Z_{eff} and n_{eff}. To adequately assess validity of results represented, I provide results for effective parameters taken from COMSOL itself to compare the results.

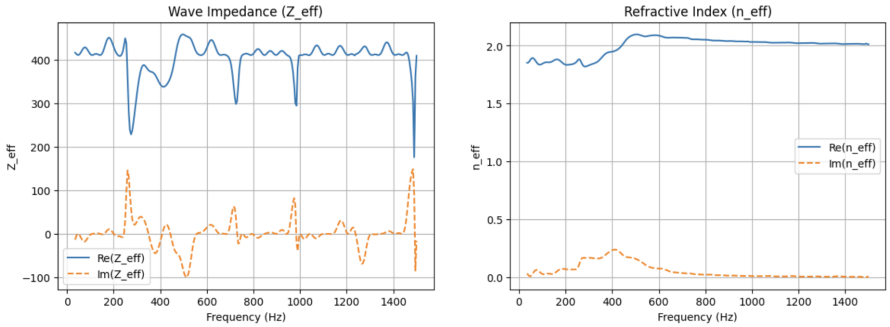

(a) Effective Acoustic Impedance (b) Effective Refractive Index

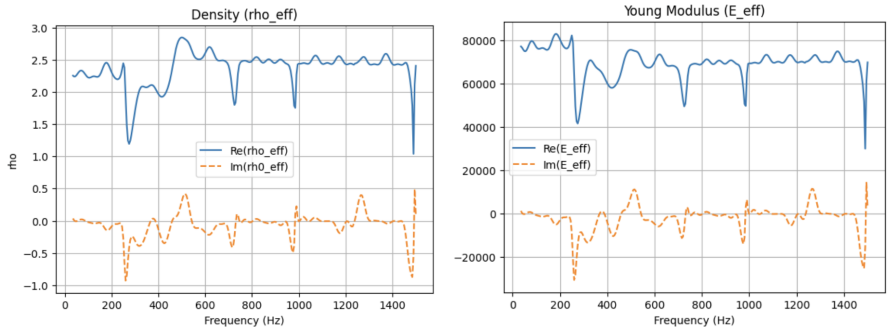

(c) Effective Density (d) Effective Young Modulus

Figure 7: Simulation with Lorentz-type Material

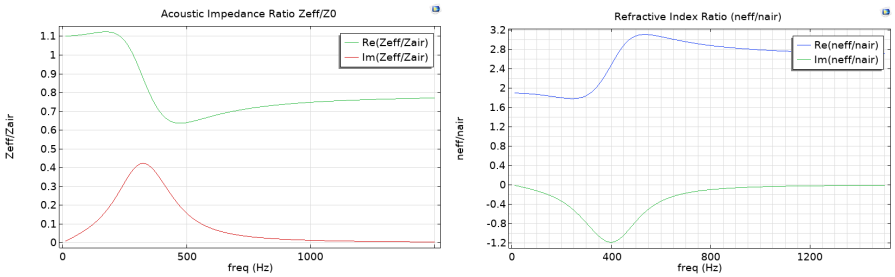

(a) Effective Acoustic Impedance (b) Effective Refractive Index

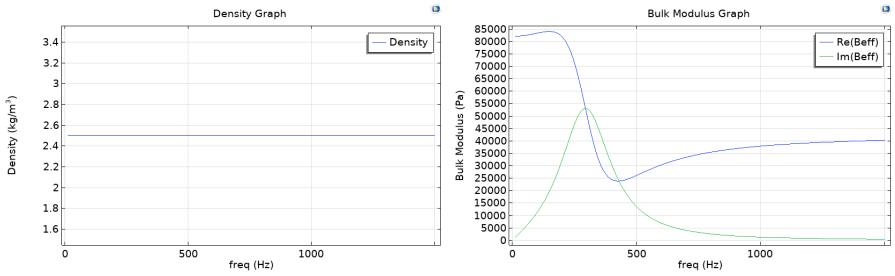

(c) Effective Density (d) Effective Young Modulus

Figure 8: COMSOL Simulation with Lorentz-type Material

In Figure 8 it is obvious that the code values are close to what is projected. However, it has sharp peaks related to improper sign choice for Z_{eff} and the branching issue with branching for n_{eff}. Ideally, our results should reiterate the COMSOL graphs.

V.2. Experiments

Initially, we derived the S parameters in empty-tube scenario to verify the quality of the waveguide. Figure 5 demonstrates that at low frequencies we have substantial noise. We have to avoid this region in our study: particularly, the noise effect is significant up to 250Hz frequency.

Therefore, we prepared Helmholtz resonators to observe resonance at approximately 580Hz. In the 400-600Hz region, we have an unusual peak at approximately 440Hz. This peak is not physical, since the S values can not go higher than 1. Thus, this peak is a result of the imperfections in the waveguide and the code. This peak occurs further in our experiments. However, it does not lie at the resonant frequency of the Helmholtz resonators, so we can disregard its effect for now. In Figure 10, results are shown for each resonator separately. As

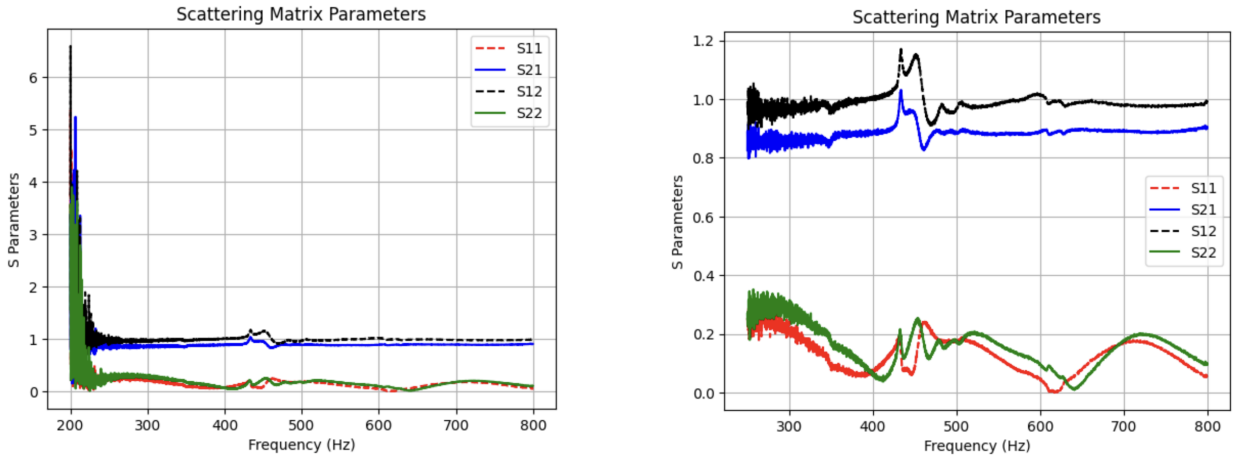

(a) S Parameters Values (200-800Hz)

(b) Cropped Version

Figure 9: Empty Tube Run

seen, all resonators have approximately the same resonant frequency. It is crucial to build them at approximately the same resonant frequencies to better observe their appearance as a locally resonant medium.

To more accurately demonstrate this evolution of a single Helmholtz resonator toward an effective medium, we made several experiments: with two, three, and four resonators connected to each other.

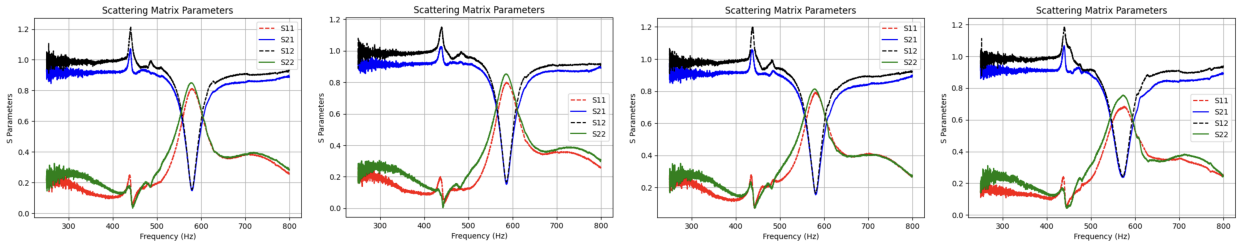

(a) (b) (c) (d)

Figure 10: Four Helmholtz Resonators

The data in Figures 12 reveals that two and three resonators together behave as resonators, yet four resonators together evolve as an effective medium with a more peculiar curve. Similarly, other values of effective parameters in the four-resonator case show discrepancy. It suggests that the aggregate effect of the resonators is not as simple as expected. Even though branching issue does not allow to obtain exact graphs, we can conclude that measurements lie within acceptable and expected range. Interestingly, the density goes to negative values mentioned in (5), which is unusual for natural materials yet possible for metamaterials.

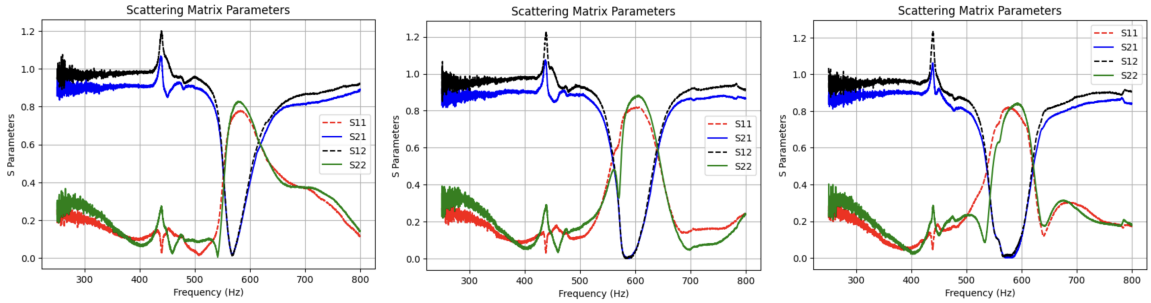

(a) Two Resonators (b) Three Resonators (c) Four Resonators

Figure 11: Resonators as Effective Medium

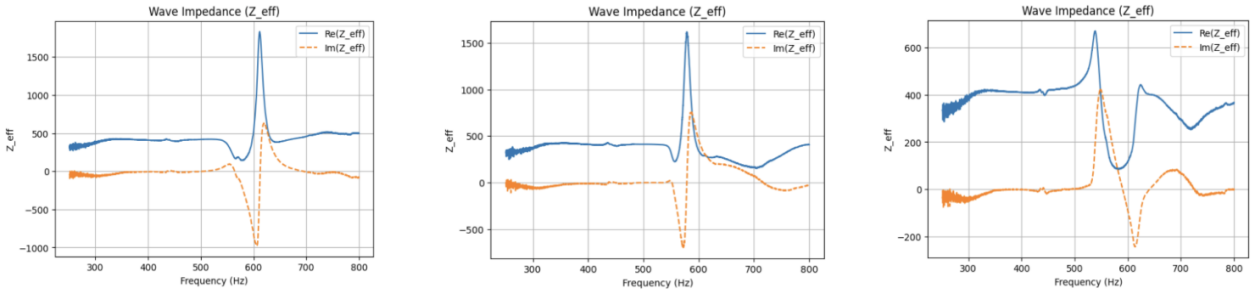

(a) Acoustic Impedance

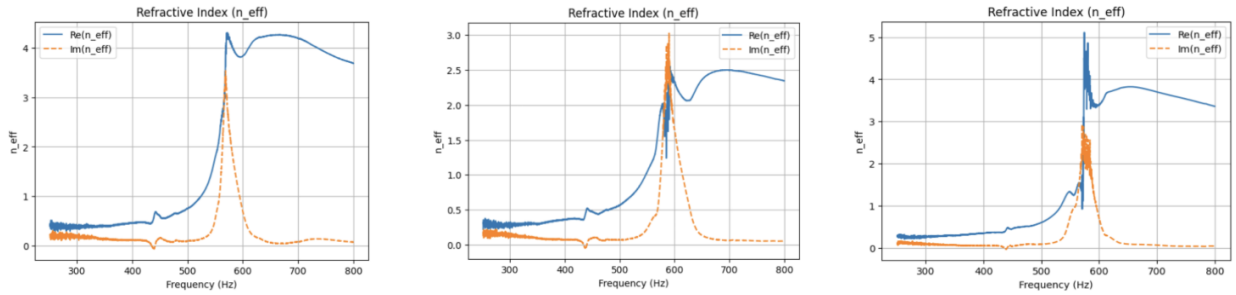

(b) Refractive Index

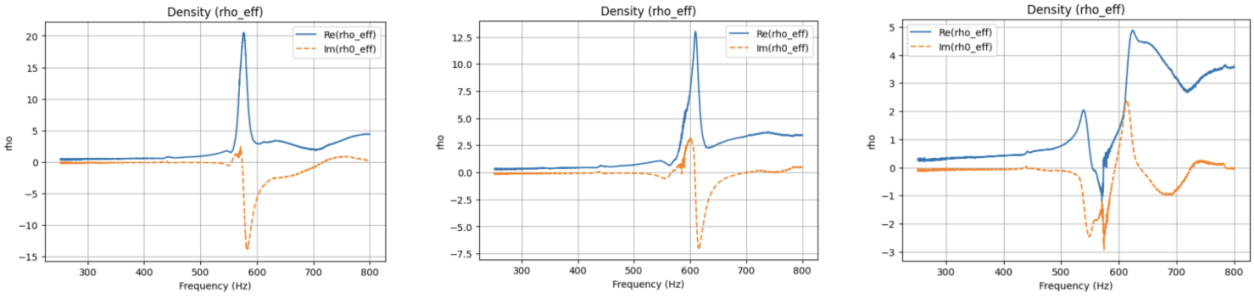

(c) Density

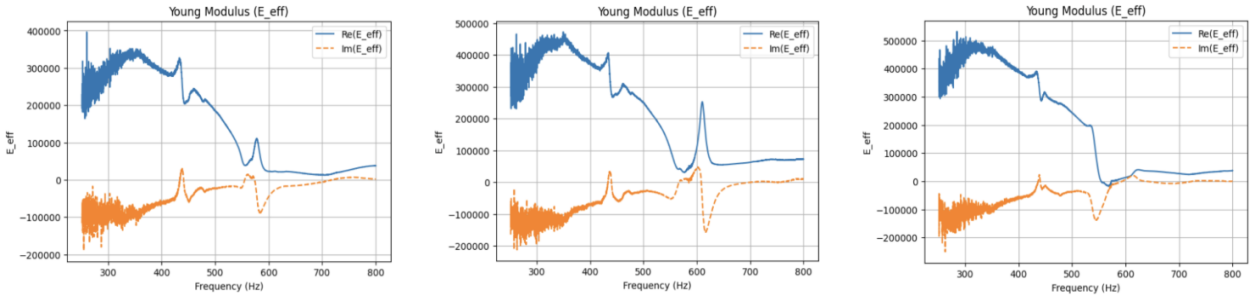

(d) Young Modulus

Figure 12: Two, Three, and Four Resonators Effective Parameters

VI. CONCLUSION

Acoustic metamaterials have the ability to demonstrate properties conventional their ability to tailor wave propagation beyond the limits of conventional media, have drawn growing attention in recent years. In this thesis we tackled one of the central bottlenecks of the acoustic metamaterials retrieving effective parameters from pressure field for dissipative samples measured inside a one-dimensional duct.

Based on NRW approach, we derived the reflection–transmission expressions for a lossy slab and added a Kramers-Kronig branch–selection rule that guarantees causal and continuous values of the complex refractive index. Once the effective impedance and refractive index are found, effective density and Young's modulus follow from the basic acoustic relations.

Based on the COMSOL simulation data reproducing the Lorentz model, we can confirm the numerical robustness of the theoretical approach. Though the graphs do not exactly repeat the simulation results due to errors in the code, found values are in a close range. Experiments with Helmholtz resonators revealed crucial resonant squeezes around 580 Hz and an in excellent agreement with the theoretical predictions. In addition, we observed the evolution of the resonators array into acoustic medium as each additional resonator significantly altered the system.

Overall, the study demonstrates that the phase-corrected extraction of S parameters is feasible and accurate for resonant acoustic structures, even when small noise is present. It is also crucial to highlight that basic acoustic metamaterials can be reproduced from locally resonant structures – as Helmholtz resonators. Even placing several resonators as an array exhibits acoustic medium properties.

Still, the present work has limitations that should be mentioned for future studies. The code we provide is not fully appropriate for the system of resonators we chose. The diameter of resonators is 5cm and can not be easily approximated as a slab. It means for future studies we have to make locally resonant structures smaller and a general number of small structures bigger.

Another potential improvement for the experimental setup might be building 2D acoustic waveguide with capacity to study more frequency modes. In this study, we have 4 detectors

in the waveguide, while in 2D acoustic waveguide we can increase microphone number up to 16. When constructing a new waveguide, it is crucial to make it transparent to control the placement of a slab.

References

[1] S. Kumar and H.-P. Lee. Recent advances in acoustic metamaterials for simultaneous sound attenuation and air ventilation performances. *Crystals*, 10(8):686, 2020.

[2] J. Zhang, B. Hu, and S. Wang. Review and perspective on acoustic metamaterials: From fundamentals to applications. *Appl. Phys. Lett.*, 123(1):010502, 2023.

[3] X. Chen, T.M. Grzegorczyk, B.-I. Wu, J. Pacheco, and J.A. Kong. Robust method to retrieve the constitutive effective parameters of metamaterials. *Phys. Rev. E*, 70(1):016608, 2004.

[4] D.R. Smith, D.C. Vier, T. Koschny, and C.M. Soukoulis. Electromagnetic parameter retrieval from inhomogeneous metamaterials. *Phys. Rev. E*, 71:036617, 2005.

[5] B. Liu, J. Zhao, X. Xu, W. Zhao, and Y. Jiang. All-angle negative reflection with an ultrathin acoustic gradient metasurface: Floquet–bloch modes perspective and experimental verification. *Sci. Rep.*, 7:13852, 2017. Accessed on: May 1, 2025.

[6] X. Chen, T.M. Grzegorczyk, B.-I. Wu, J. Pacheco Jr., and J.A. Kong. Robust method to retrieve the constitutive effective parameters of metamaterials. *Phys. Rev. E*, 70(1):016608, 2004.

[7] S. Shi, X. Qiao, S. Liu, and W. Liu. Retrieval of the effective constitutive parameters from metamaterial absorbers. *Chin. Phys. B*, 30(11):117803, 2021.

[8] J. Li and C.-T. Chan. Double-negative acoustic metamaterial. *Phys. Rev. E*, 70:055602, 2004.

[9] G. Ma and P. Sheng. Acoustic metasurfaces: From localized resonances to broad horizons. *Sci. Adv.*, 2(2):e1501595, 2016.

[10] W.B. Weir. Automatic measurement of complex dielectric constant and permeability at microwave frequencies. *Proc. IEEE*, 62(1):33–36, 1974.

[11] J.U. Satti. *Scattering Analysis of Acoustic Waves in Waveguides Containing Partitioned Wave-Bearing Cavities*. Ph.d. thesis, Capital University of Science and Technology, Islamabad, Pakistan, 2021. Accessed on: May 1, 2025.

[12] S. Rodriguez, V. Gibiat, A. Lefebvre, and S. Guilain. The three-measurement two-calibration method for measuring the transfer matrix. In *Proc. Meet. Acoust.*, vol-

ume 107, pages 1131–1152, 2000.

[13] X. Chen, T.M. Grzegorczyk, B.-I. Wu, J. Pacheco, and J.A. Kong. Robust method to retrieve the constitutive effective parameters of metamaterials. *Phys. Rev. E*, 70(1):016608, 2004.

[14] D.R. Smith, D.C. Vier, T. Koschny, and C.M. Soukoulis. Electromagnetic parameter retrieval from inhomogeneous metamaterials. *Phys. Rev. E*, 71:036617, 2005.

[15] V.V. Varadan and R. Ro. Unique retrieval of complex permittivity and permeability of dispersive materials from reflection and transmitted fields by enforcing causality. *IEEE Trans. Microw. Theory Techn.*, 55(10):2224–2230, 2007.

[16] G. Lubkowski, R. Schumann, and T. Weiland. Extraction of effective material parameters by parameter fitting of dispersive models. *Microw. Opt. Technol. Lett.*, 49(2):285–288, 2007.

[17] Z. Szabó, G.-H. Park, R. Hegde, and E.-P. Li. A unique extraction of metamaterial parameters based on kramers–kronig relationship. *IEEE Trans. Microw. Theory Techn.*, 58(10):2646–2657, 2010.

[18] K.E. Peiponen, V. Lucarini, E.M. Vartiainen, and J.J. Saarinen. Kramers–kronig relations and sum rules of negative-index media. *Eur. Phys. J. B*, 41:61–65, 2004.

[19] S.A. Cummer, J. Christensen, and A. Alù. Controlling sound with acoustic metamaterials. *Nat. Rev. Mater.*, 1(3):16001, 2016.

[20] N. Fang, D. Xi, J. Xu, M. Ambati, W. Srituravanich, C. Sun, and X. Zhang. Ultrasonic metamaterials with negative modulus. *Nat. Mater.*, 5:452–456, 2006.

[21] J. Li and C.-T. Chan. Double-negative acoustic metamaterial. *Phys. Rev. E*, 70:055602(R), 2004.

[22] V. Fokin, M. Ambati, C. Sun, and X. Zhang. Method for retrieving effective properties of locally resonant acoustic metamaterials. *Phys. Rev. B*, 76:144302, 2007.

[23] M. Ambati, N. Fang, C. Sun, and X. Zhang. Surface resonant states and superlensing in acoustic metamaterials. *Phys. Rev. B*, 75:195447, 2007.

[24] F. Cervera, L. Sanchis, J.V. Sánchez-Pérez, R. Martínez-Sala, C. Rubio, F. Meseguer, C. López, D. Caballero, and J. Sánchez-Dehesa. Refractive acoustic devices for airborne sound. *Phys. Rev. Lett.*, 88(2):023902, 2001.

[25] M.L. Munjal. *Acoustics of Ducts and Mufflers with Application to Exhaust and Ventilation System Design*. Wiley-Interscience, New York, NY, USA, 1987.

[26] P. Li, S. Yao, X. Zhou, G. Huang, and G. Hu. Effective medium theory of thin-plate acoustic metamaterials. *J. Acoust. Soc. Am.*, 135(4):1844–1852, 2014.

[27] C.G. Parazzoli, R.B. Greegor, and M.H. Tanielian. Development of negative-index metamaterials for rf lens applications. In C.M. Krowne and Y. Zhang, editors, *Physics of Negative Refraction and Negative Index Materials*, pages 261–329. Springer, Boston, MA, USA, 2007.

[28] C. Menzel, C. Rockstuhl, T. Paul, F. Lederer, and T. Pertsch. Retrieving effective parameters for metamaterials at oblique incidence. *Phys. Rev. B*, 77:195328, 2008.

Appendix

A. Python Code to Extract S Matrix

```
def Smat_extract(Nm, fc, x, a, dz, pm):
    exc = np.ones(2 * Nm)
    pexc = np.diag(exc)
    c_speed = 343  # speed of sound at 25 deg C
    if fc == 0:
        print("Zero frequency, singular scattering matrix")
        fc = 0.1

    # calculate coefficients
    ky = np.array([(aa) * np.pi / a for aa in range(Nm)])
    kz = np.sqrt((2 * np.pi * fc / c_speed)**2 - ky**2)
    # calculate fy
    fy = np.array([[np.cos(ky_val * x_val) for x_val in x] for ky_val in ky])

    # write matrix
    z1 = 0
    z2 = z1 + dz
    c_matrix = fy * np.exp(-1j * kz[:, None] * z1)
    d_matrix = fy * np.exp(1j * kz[:, None] * z1)
    g_matrix = fy * np.exp(-1j * kz[:, None] * z2)
    h_matrix = fy * np.exp(1j * kz[:, None] * z2)
    z = np.zeros((len(x), Nm))

    m1 = np.block([[c_matrix, z], [g_matrix, z], [z, c_matrix], [z, g_matrix]])
    m2 = np.block([[d_matrix, z], [h_matrix, z], [z, d_matrix], [z, h_matrix]])
```

```
m = np.concatenate((m1, m2), axis=1)
pm = pm.reshape(4*Nm, 2*Nm)

# Validate the shape of pm
if pm.shape != (4 * Nm, 2 * Nm):
    raise ValueError(f"Shape of pm is {pm.shape}, but expected (4*Nm, 2*Nm)")

AB = None

try:
    # First, attempt to solve the system with a generic solver (you'll need to defin
    AB = solve(m, pm)
except Exception as e:
    print(f"Generic solver failed: {e}")
    try:
        # If the generic solver fails, try using NumPy's least squares solver
        AB = np.linalg.lstsq(m, pm, rcond=None)[0]
    except np.linalg.LinAlgError as e:
        print(f"Least squares failed: {e}")
        try:
            # If least squares fail, try using the pseudo-inverse
            pseudo_inverse = np.linalg.pinv(m)
            AB = np.dot(pseudo_inverse, pm)
        except np.linalg.LinAlgError as e:
            print(f"Pseudo-inverse failed as well: {e}")
            # At this point, all methods have failed. Handle accordingly.

# Check if AB was successfully computed
if AB is None:
    # print("Solution found using one of the methods.")
```

```
        print("No solution found using any method.")

    # solve for each mode
    A = AB[:2 * Nm, :]
    B = AB[2 * Nm:4 * Nm, :]
    A_inv = inv(A)
    S = np.dot(B, A_inv)
    M = np.dot(pexc, A_inv)

    return S, M, AB
```

B. Python Code to Retrieve Effective Parameters

```
def adjusting_R_T(freq, S11, S21):
  omega = 2.0 * np.pi * freq
  k0 = omega / speed_c

  S11_real = np.real(S11)
  S11_imag = np.imag(S11)
  S21_real = np.real(S21)
  S21_imag = np.imag(S21)

  # Compute magnitude & phase (unwrapped)
  S11_abs = np.abs(S11)
  S11_phase = np.unwrap(np.angle(S11))
  S21_abs = np.abs(S21)
  S21_phase = np.unwrap(np.angle(S21))
```

```
  # Reference-plane correction
  # Multiply by exp(-j*k0*(2*ref1)) or exp(-j*k0*(ref1+ref2)).
  #R = S11_abs * np.exp(-1j * S11_phase) * np.exp(-1j *  k0  * (2*ref1-d_eff))
  #T = S21_abs * np.exp(-1j * S21_phase) * np.exp(-1j * k0 *  (ref1 + ref2 - d_eff))
  R = S11_abs * np.exp(-1j * S11_phase) * np.exp(-1j * k0 * 2.0 * ref1)
  T = S21_abs * np.exp(-1j * S21_phase) * np.exp(-1j * k0 * (ref1 + ref2))
  return R, T

  from scipy.integrate import trapezoid
def retrieve_Z_n(freq, R, T):
    Z_0 = 343*1.2
    omega = 2.0 * np.pi * freq
    k0 = omega / speed_c
    m_max =5
    tol = 1e-2
    d_eff = 0.343
    branch_search_range = 5
    # Prepare arrays to hold final, continuity-corrected values
    N = len(freq)
    Z_eff_raw = np.zeros(N, dtype=complex)
    Z_eff_raw = Z_0*(((1+R**2)**2-T**2)/((1-R**2)**2-T**2))**0.5
    exp_ink0d_raw = T / (1 - R * (Z_eff_raw-Z_0)/(Z_eff_raw+Z_0))



    Z_eff = np.zeros(N, dtype=complex)
    exp_ink0d = np.zeros(N, dtype=complex)
    n_eff = np.zeros(N, dtype=complex)
    n_candidate = np.zeros(N, dtype=complex)
    #Decide the sign of Z_eff[i] to keep Re(Z_eff) or magnitude continuity
    #This logic is from your original "choose sign" approach
```

```
for i in range(N):
    # 4A) Decide the sign of Z_eff[i] to keep Re(Z_eff) or magnitude continuity
    #     This logic is from your original "choose sign" approach
    Zcandidate = Z_eff_raw[i]
    reZ = np.real(Zcandidate)
    if np.abs(reZ) > tol:
        # Flip sign if reZ < 0
        if reZ < 0:
            Zcandidate = -Zcandidate
            expCandidate = (
                T / (1 - R * (Z_eff_raw-Z_0)/(Z_eff_raw+Z_0))
            )
        else:
            expCandidate = exp_ink0d_raw[i]
    else:
        # If real(Z_eff) is very small, check magnitude of exp(ink0d)
        if np.abs(exp_ink0d_raw[i]) > 1.0:
            Zcandidate = -Zcandidate
            expCandidate = (
                T / (1 - R * (Z_eff_raw-Z_0)/(Z_eff_raw+Z_0))
            )
        else:
            expCandidate = exp_ink0d_raw[i]

    Z_eff[i] = Zcandidate
    exp_ink0d[i] = expCandidate
    logExp = np.log(expCandidate)
    n_candidate[i] = (np.imag(logExp) - 1j * np.real(logExp)) / (k0[i] * d_eff)
```

```
# ------------------------------------------------------------------
# 1) Kramers-Kronig (discrete) estimate of Re{n}.
#    n_im = Im{n_candidate} is used directly.  Principal value is
#    handled by skipping the i=j term in the trapezoidal sum.
# ------------------------------------------------------------------
n_im = np.imag(n_candidate)
n_re_KK = np.empty_like(n_im)

# frequency increment array (finite differences)
df = np.gradient(freq)

for i,fi in enumerate(freq):
    # Denominator (_j^2-_i^2)  /!\   Avoid j=i !
    num   = omega * n_im              # vector
    denom = omega**2 - omega[i]**2
    denom[i] = np.inf             # forces term i=i to zero
    integrand = num/denom
    # Trapezoidal integration in -domain
    KK_int = trapezoid(integrand, omega)
    n_re_KK[i] = (2/np.pi)*KK_int

# ------------------------------------------------------------------
# 2) Branch selection: choose integer m so that
#    Re{ n_c + m*n }  n_re_KK     with n = 2/(k0 d)
# ------------------------------------------------------------------
n   = 2.0*np.pi/(k0 * d_eff)      # n is real & freq-dependent
n_eff  = np.empty_like(n_candidate)
m_vals = np.zeros(N, dtype=int)

for i in range(N):
```

```
    dn = n[i]
    # trial shifts for m in [-m_max ... +m_max]
    m_range = np.arange(-m_max, m_max+1)
    candidates = n_candidate[i] + m_range*dn
    idx_best   = np.argmin(np.abs(np.real(candidates) - n_re_KK[i]))
    n_eff[i]   = candidates[idx_best]
    m_vals[i]  = m_range[idx_best]

r0_eff = np.conj(Z_eff*n_eff)/speed_c
E_eff  = np.conj(Z_eff*speed_c)/n_eff
return  Z_eff, n_eff, r0_eff, E_eff
```